Anomalous approach to thermodynamic equilibrium: Structure formation of molecules after vapor deposition

Pritam Kumar Jana
Westfälische Wilhelms Universität Münster, Institut für Physikalische Chemie, Corrensstrasse 30, 48149 Münster, Germany

Can Wang
Westfälische Wilhelms Universität Münster, Physikalisches Institut, Wilhelm-Klemm-Strasse 10, 48149 Münster, Germany

Robert L. Jack
Department of Physics, University of Bath, Bath BA2 7AY, United Kingdom

Lifeng Chi
Westfälische Wilhelms Universität Münster, Physikalisches Institut, Wilhelm-Klemm-Strasse 10, 48149 Münster, Germany and Institute of Functional Nano & Soft Materials (FUNSOM), Soochow University, 215123 Suzhou, Jiangsu, China

Andreas Heuer*
Westfälische Wilhelms Universität Münster, Institut für Physikalische Chemie, Corrensstrasse 30, 48149 Münster, Germany and Center of Nonlinear Science CeNoS, Westfälische Wilhelms Universität Münster, Germany

(Received 11 April 2015; revised manuscript received 23 August 2015; published 16 November 2015)

We describe experiments and computer simulations of molecular deposition on a substrate in which the molecules (substituted adenine derivatives) self-assemble into ordered structures. The resulting structures depend strongly on the deposition rate (flux). In particular, there are two competing surface morphologies (α and β), which differ by their topology (interdigitated vs lamellar structure). Experimentally, the α phase dominates at both low and high flux, with the β phase being most important in the intermediate regime. A similar nonmonotonic behavior is observed on varying the substrate temperature. To understand these effects from a theoretical perspective, a lattice model is devised which reproduces qualitatively the topological features of both phases. Via extensive Monte Carlo studies we can, on the one hand, reproduce the experimental results and, on the other hand, obtain a microscopic understanding of the mechanisms behind this anomalous behavior. The results are discussed in terms of an interplay between kinetic trapping and temporal exploration of configuration space.

DOI: 10.1103/PhysRevE.92.052402 PACS number(s): 68.43.Hn, 05.10.−a, 05.65.+b, 68.37.Ef

I. INTRODUCTION

Understanding the structure formation of organic molecules on surfaces is of major interest due to its technological importance [1], e.g., for organic thin-film transitions [2–4] or organic-light-emitting diodes [5]. Key advantages of organic molecules are related to their ease of processing and their flexibility [6]. In many experimental realizations the molecules are deposited on the substrate via appropriate deposition procedures. Thus the resulting structures are formed in a nonequilibrium setting [7]. Modelling such nonequilibrium systems is an ongoing challenge in physics. One smart way to generate desired structures is to use prepatterned substrates [8–10]. Subtle orientation effects may result from the anisotropy of the adsorbate [11]. On bare substrates one may ask, e.g., for the properties of nucleation events [7] and, e.g., its dependence on the anisotropy of the molecular interaction [12]. Naturally, the characteristics of the substrate also have an impact on the structural order of the thin films [13].

From a theoretical perspective an important question deals with the dependence of the resulting structure on deposition rate, i.e., the flux of molecules on the substrate. The limit of zero flux can be described by equilibrium concepts (at least for finite systems), but nonequilibrium effects are inevitable as soon as the flux is nonzero. Ultrastable glasses [14] constitute one class of interesting system, where the flux dependence has been studied. It has been shown experimentally for indomethacin that the enthalpy of the resulting structures monotonically depends on the chosen flux: the lower the flux the lower the enthalpy [14]. In different experiments it has been shown that a higher flux generates a higher nucleation density and smaller average grain sizes [6].

In this context we have recently presented experiments on deposition of certain organic molecules (specifically, substituted adenine derivatives A-C22 with an alkyl chain containing 22 carbon atoms) [15]. When studying the resulting structure after the growth of one monolayer, two different phases (denoted α and β) were identified via analysis of scanning tunneling microscopy (STM) images. In the α phase, adenine nucleobases lie flat on the surface and form intermolecular hydrogen bonds, denoted as α bonds in later discussions; in the β phase the adenine molecules are tilted out of the plane and are expected to interact via a $\pi - \pi$ interaction between adenine aromatic rings (these are denoted as β bonds). In these experiments it has been observed that for low substrate temperatures (at fixed flux) the α phase is predominantly formed. Furthermore, in previous solution phase experiments at low temperatures mainly the α phase is observed. This suggests,

*Corresponding author: andheuer@uni-muenster.de

consistent with the corresponding theoretical analysis [16], that the α phase is the thermodynamically stable phase at low temperatures.

However, the dependence of the experimental results on the deposition rate was unexpected: it was found that lower flux led to a larger contribution of the metastable β phase [15]. Similar effects were reproduced in Monte Carlo (MC) simulations, based on a model of molecules moving on a lattice. In this paper we show results of experiments and MC results which demonstrate other, more complex, nonequilibrium effects in this system. For an appropriately chosen flux we experimentally observe a nonmonotonous dependence on temperature: the α phase dominates at both low and high temperatures, while for intermediate temperatures one observes a surplus of the β phase. The MC simulation results demonstrate that this anomalous behavior can be explained through the different topology of the α phase (interdigitated structure) and the β phase (lamellar structure). This topology has implications for the growth of these phases. We also discuss our results in the context of different theoretical results, previously reported in the literature, about complex nonequilibrium effects in the growth of molecular aggregates, and kinetic trapping effects.

II. MODEL AND SIMULATION DETAILS

A. Definition of the lattice model

We first define the lattice MC model that we use in our simulations. As illustrated in Fig. 1, we mimic the organic molecule used in experiments by a rigid chain which consists of five beads: one head (H) and four tail (T) beads. We consider a square lattice of length $L = 101$ with periodic boundary conditions in both directions, where each bead occupies one lattice site. The total number of chains after deposition is $N = 1600$, corresponding to a maximum coverage of approximately 80%. Any overlap of the chains is forbidden.

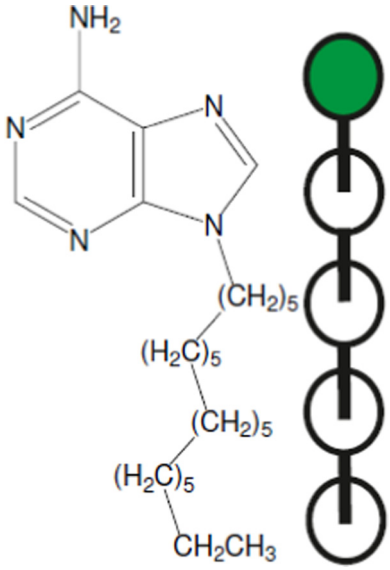

FIG. 1. (Color online) The comparison of (a) the substituted adenine molecule A-C22 and (b) a model chain where the head bead is shown in green and the four tail beads in white.

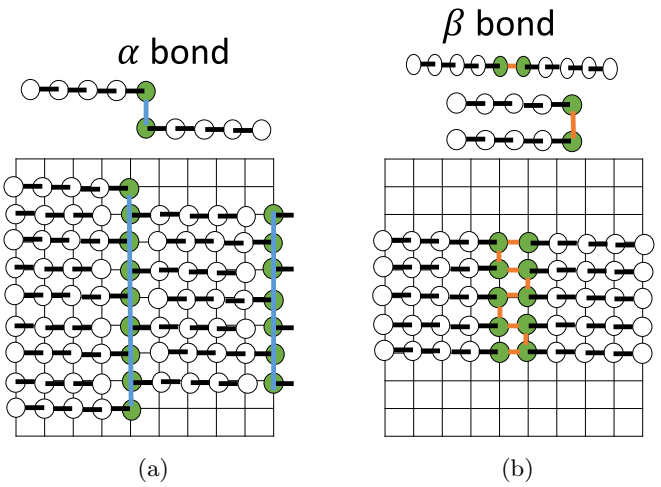

FIG. 2. (Color online) Construction of (a) the interdigitated α and (b) the lamellar β phase with the lattice model. The possible bonds are highlighted on top.

The simulations performed in this work involve averages of up to 400 independent runs per parameter set.

The model is designed to support the formation of the two phases observed experimentally. As mentioned above, the α phase corresponds to an interdigitated network structure and the β phase to a lamellar structure. The respective topologies within the model are shown in Fig. 2. The interaction energy among molecules consists of a sum over all adjacent pairs of particles which do not belong to the same chain. The pair interactions depend on the type of particle (head or tail) and on the relative orientations of the relevant molecules. For the interaction of two tail particles, occupying two nearest-neighbor sites, two cases have to be distinguished. First, the corresponding chains are parallel and the connecting vector between both particles is orthogonal to the vector along the chains. Then the interaction is strongest with an energy denoted as u_{TT}. Second, if either of the chains are orthogonal to each other or both chains are aligned along the same line in an antiparallel fashion, a smaller interaction energy $u_{\tilde{T}T}$ is present. The interaction between head and tail particles is u_{HT}. All interaction energies are also shown in Fig. 3.

To stabilize the configurations depicted in Fig. 2, we introduce bonds which reflect the hydrogen bonds and the $\pi - \pi$-stacking in the experimental system. These bonds are direction-dependent and may be made and broken during the MC simulation. To form an α bond between two head groups, two adjacent chains have to be arranged as shown in the top part of Fig. 2. In β bonds, there are two cases: either (i) the two chains are antiparallel with each other and the bond is parallel to the chains, or (ii) the two chains are parallel with each other and the bond is perpendicular to both chains. The two situations are shown in Fig. 2. If a chain participates in two β bonds, then one bond must be parallel and one perpendicular to the chain itself. Chains may participate in up to two β bonds or up to two α bonds, but no chain may simultaneously participate in both α and β bonds.

These bonds are accounted for by extra degrees of freedom in the system, so an adjacent pair of head particles may be either bound or unbound. If the particles are not bound then

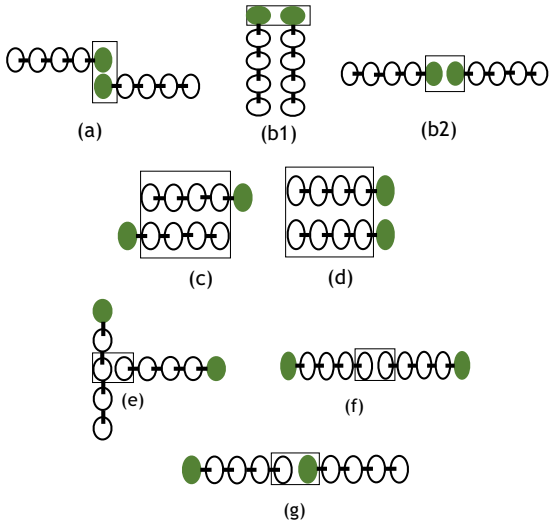

FIG. 3. (Color online) The different terms, listed in Table I: (a) $u_{HH,\alpha}$, (b) $u_{HH,\beta}$, (c) and (d) u_{TT} for different orientations of adjacent chains, (e) and (f) $u_{\tilde{T}T}$ for different orientations of adjacent chains, and (g) u_{HT}.

their interaction energy is zero; if they are bound the interaction energy is $u_{HH,\alpha}$ or $u_{HH,\beta}$, according to the type of bond.

The interaction energies are fixed throughout this work and are tabulated in Table I. The parameters $u_{HH,\alpha}$, u_{TT}, and $u_{\tilde{T}T}$ are taken from the previous density functional theory (DFT) calculations [16]. The DFT calculations did not allow the estimation of $u_{HH,\beta}$ due to the more complex binding situation (see above). However, previous experiments suggest [15,16] that in equilibrium the α phase is the thermodynamically stable state at low temperatures. Thus we choose in the present model the binding energy of the β bond somewhat smaller than that of the α bond. Specifically, we choose $u_{HH,\beta} = -0.34$ eV. (The qualitative results of this paper do not depend on this specific choice.) To choose the value of u_{HT}, we imagine the (artificial) case $u_{HH,\alpha} = u_{HH,\beta} = -0.5$ eV and we choose u_{HT} such that the pure α and β phases would (in that case) have the same potential energy per chain, in the thermodynamic limit.

B. Monte Carlo algorithm

The time evolution of this system is governed by a Monte Carlo algorithm. On each Monte Carlo time step, all chains are selected in a random order. All time scales (e.g., inverse flux) in this work are expressed in terms of this Monte Carlo time step. For each chain, three types of analysis are performed. (1) If a chain with a single bond is selected, this bond is opened with probability $\exp(-u_{HH,i}/k_BT)$ ($i \in \{\alpha,\beta\}$). (2) If this chain has no bond (either because it was opened or because it was already unbound), we attempt a translational and a rotational move. During a translational motion a chain is moved by a single lattice site and the direction of the motion is selected randomly. During a rotational motion a chain is rotated along the head and the end bead in a systematic way by an angle of 90°, in a randomly chosen direction. The acceptance of this step is analyzed via the standard Metropolis criterion where the energetic contributions of the HT and TT interaction are taken into account. In case of a possible overlap this move is naturally not accepted. (3) A bond is formed between this chain and another chain whenever it is compatible with the bond criteria defined above.

In addition to the motion of the chains, every $1/F$ time steps a new chain is randomly deposited on the surface. If this step fails due to some resulting overlap, it is rejected and tried again until the proposed chain position is accessible. The value of F denotes the incoming particle flux. Since the interaction energies are fixed throughout the simulation, the relevant parameters for comparison with experiments are the particle flux F and the substrate temperature T.

The inclusion of explicit bonds within this model makes it somewhat more complicated than a conventional MC simulation where the energy depends only on the configuration of the molecules (and not on the bonds). However, the algorithm used here separates the opening of a temporary bond and the motion of the molecules. In this way the model dynamics more closely resembles the actual physicochemical processes that occur in the experimental system. From Fig. 2, note also that there may be more than one arrangement of bonds that is consistent with a given configuration of the molecules. For a precise formulation of the model, we specify the state of the system in terms of the number of molecules, their positions and orientations, and the locations (and types) of all α and β bonds. The system energy is a single-valued function of all these coordinates, and the acceptance probabilities for molecular moves in our Monte Carlo scheme are then given by the standard Metropolis formula.

Note, however, that events where particles form two bonds simultaneously can sometimes occur within the dynamical scheme, but the reverse procedure in which two bonds are broken simultaneously is not allowed. This means that while the scheme is simple, there are some violations of detailed balance. However, the acceptance probabilities for events in which two bonds are broken are extremely small, due both to the small Metropolis factor and to crowding effects which hinder movement for molecules that already have two bonds. Since these events are very rare and have a very weak effect on the dynamics, we therefore choose to neglect them. Of course, the events where particles are added to the system also break detailed balance, consistent with the nonequilibrium nature of the vapor deposition experiment. However, in the limit of slow deposition ($F \to 0$), the density of particles changes so slowly so that the system has time to equilibrate at the substrate temperature in between successive particle addition. In this case the deposition is a thermodynamically reversible isothermal process: it is also a quasiequilibrium assembly in the sense of [17].

TABLE I. Interaction energies used in the simulation in units of electronvolts.

Pair		Interaction potential
HH	$u_{HH,\alpha}$	–0.50
	$u_{HH,\beta}$	–0.34
TT	u_{TT}	–0.10
	$u_{\tilde{T}T}$	–0.032
HT	u_{HT}	–0.016

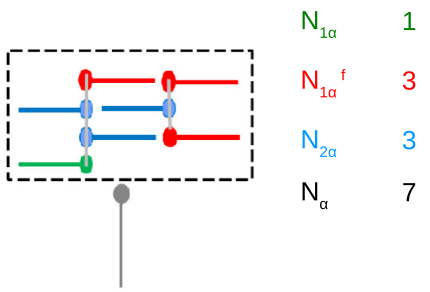

FIG. 4. (Color online) An example to display the definition of a chain with single bonds [free (red) and nonfree (green)] and two bonds (blue).

C. Analyzing the structure of growing clusters

For the detailed analysis in this work we need to quantify the amounts of α and β phase in the system (see Fig. 4). We use $N_{2\alpha}$ to denote the number of chains with two α bonds. For chains with just a single α bond we distinguish "free chains," the number of which is $N_{1\alpha}^{f}$, and "blocked chains," the number of which is $N_{1\alpha}$. Free chains are those that are available for α bonding. In practice this means either (a) that it is possible to introduce a new chain which forms a second α bond with the free chain (without obstruction by another chain nearby) or (b) that a chain near to the free chain can form an α bond with it by a single MC move (translation or rotation). If neither of these conditions is met, then the chain is "blocked."

The total number of α-bonded chains is $N_\alpha = N_{2\alpha} + N_{1\alpha}^{f} + N_{1\alpha}$; similarly, the total number of β-bonded chains is N_β. In the following, we mainly analyze the characteristics of chains forming α bonds—interactions are strong in this system at the temperatures considered, so chains that do not form α bonds have (in most cases) already formed β bonds.

III. EXPERIMENTS

A. Methods

STM experiments were performed by using a commercial multimode nanoscope scanning tunneling microscope (Digital Instruments Co., Santa Barbara, CA) with mechanically cut Pt-Ir (90:10) tips at ambient temperature. For preparation, A-C22 was deposited by vacuum sublimation onto a freshly cleaved surface of highly orientated pyrolytic graphite (HOPG, MaTech GmbH) for 20 min. Then the STM measurements were performed, and the images shown were recorded in constant-current mode at the air–substrate interface. Different tips and samples were used to check for reproducibility and to ensure that there are no image artifacts caused by the tips or samples. The parameters, varied in the different experiments, are the substrate temperature and the evaporation temperature. The latter temperature controls the flux of molecules on the substrate.

B. STM image for high substrate temperature

In Fig. 5 three large-scale constant-current STM images are shown for different substrate temperatures, varying between 318 and 363 K. The evaporation temperature is fixed. Careful analysis of the data suggests, in agreement with previous work [15], that there are two types of structures with different stripe widths. The narrower stripes correspond to the α phase, the wider stripes to the β phase. From counting the fraction of both phases, one sees that the amount of the α phase first decreases and then increases when increasing the substrate temperature.

IV. RESULTS

A. Overall flux and temperature dependence

In Fig. 6 we compare experimental and numerical results. The first row shows the fraction of the α phase as a function of substrate temperature T. The second and third rows show similar results as a function of flux (or, equivalently, inverse evaporation temperature) at two different substrate temperatures. The results of the simulations are obtained for a coverage of $\Theta = 0.8$.

In the temperature regime $T \leqslant 333$ K, analyzed in Ref. [15], the dependence on temperature was consistent with the behavior that is expected on intuitive grounds. That is, increasing the substrate temperature reduced the "yield" of the stable α phase, so $N_\alpha/N_{\rm tot}$ decreases monotonically with increasing substrate temperature. In the results shown here, the (substrate) temperature regime was increased to 363 K, which reveals a nonmonotonicity in $N_\alpha/N_{\rm tot}$: at high temperature, the yield is an increasing function of T. This is the first indication of unusual nonequilibrium effects in this system.

Turning to the flux dependence of $N_\alpha/N_{\rm tot}$, two different regimes can be identified. For low substrate temperatures,

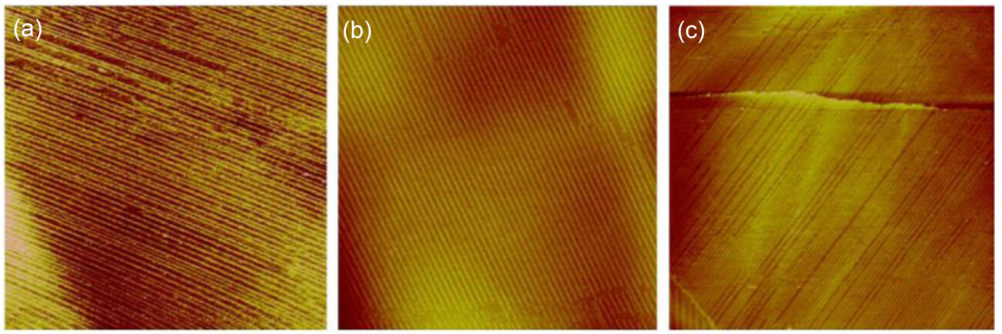

FIG. 5. (Color online) Large-scale STM constant-current images of A-C22 physisorbed onto a graphite surface by evaporation (250 × 250 nm). Fixed evaporation temperature is 383 K. (a) $T_{sub} = 318$ K, $V_{bias} = -1.170$ V, $I_{set} = 0.100$ nA; (b) $T_{sub} = 333$ K, $V_{bias} = -0.886$ V, $I_{set} = 0.100$ nA; (c) $T_{sub} = 363$ K, $V_{bias} = -1.64$ V, $I_{set} = 0.901$ nA.

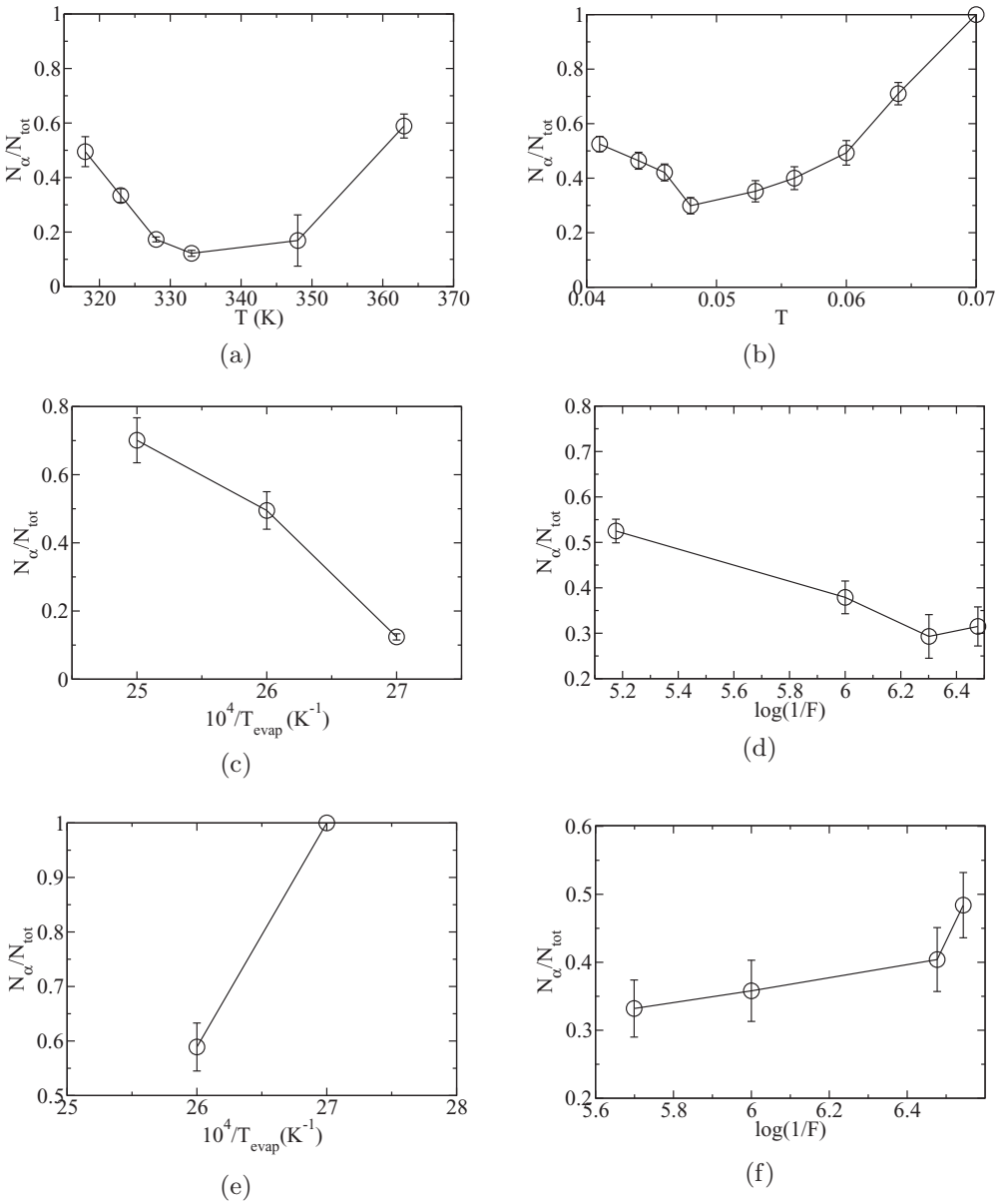

FIG. 6. $N_{\alpha,\beta}/N_{\text{tot}}$ as a function of substrate temperature and either evaporation temperature (left) or deposition rate (right). Left column: experiment; right column: simulations. (a) Fixed evaporation temperature (i.e., deposition rate) $T_{\text{evap}} = 383$ K and (b) fixed deposition rate $F = 6.7 \times 10^{-6}$. Fixed substrate temperatures (c) $T = 318$ K and (d) $T = 0.041$. Somewhat larger substrate temperatures (e) $T = 363$ K and (f) $T = 0.057$.

reducing the particle flux reduces the yield of the stable α phase, contrary to the intuitive expectation that a reduction of the flux should promote equilibrium behavior. Similar data were already shown in Ref. [15]. Moreover, we show here that experimental and simulation results at higher substrate temperatures interestingly yield the opposite flux dependence to those at low temperature. This high-temperature result corresponds to the expected behavior that reduced flux promotes the equilibrium stable phase.

Naturally, in the limit of infinitesimally slow flux the system should approach its equilibrium state. The enthalpy of a pure α phase, expressed as the energy per chain, is -0.916, as compared to the corresponding β-phase value of -0.756. Making a naive estimate based on Boltzmann weights and neglecting possible interaction effects between both phases, one expects that for equilibrium at $T = 0.041$ one has $N_\alpha/N_{\text{tot}} \approx 0.98$. (In fact, this is expected to be an underestimate due to correlations between molecules.) Thus, for all flux values shown in Fig. 6(d), one observes much less of the α phase than would be expected at equilibrium.

Clearly, the dynamical behavior of this system is quite complex. However, all of the experimental behavior in Fig. 6 are mirrored (qualitatively) by the Monte Carlo simulations. In the remainder of this work, we explore these effects in more detail.

B. Understanding the dependence of N_α/N_{tot} on coverage

We start by considering conditions ($T = 0.041$, $F = 6.7 \times 10^{-6}$), where both α and β form at almost equal amounts.

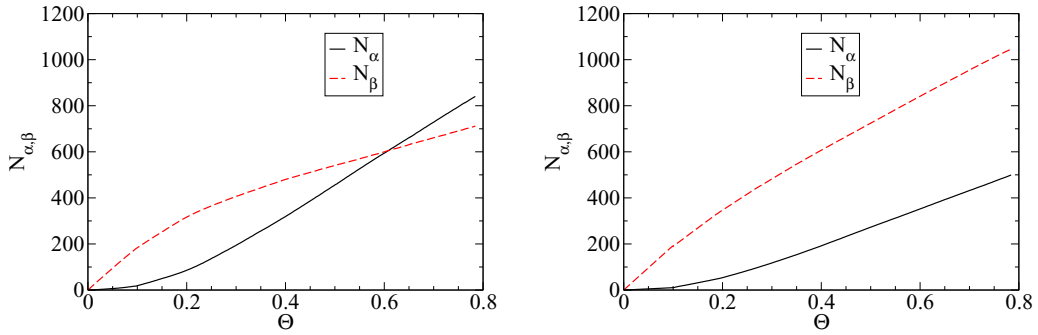

FIG. 7. (Color online) $N_{\alpha,\beta}$ as a function of coverage Θ at fixed deposition rate (a) $F = 6.7 \times 10^{-6}$ and (b) $F = 3.3 \times 10^{-7}$ at temperature $T = 0.041$.

Figure 7 shows $N_{\alpha,\beta}$ as a function of coverage Θ, which is proportional to the time since the start of deposition. Two important features can be seen. For very low coverage there is a dramatic difference between N_β and N_α. For example, at $\Theta = 0.05$ they differ by a factor of $\sim$15. This result already gives a clue as to the dominant kinetic effect in this system.

The origin of this effect is the different topology of the phases, as shown in Fig. 2. Two chains side by side in the β configuration are stabilized by attractive interactions between their tail particles, and further growth of these clusters is now favorable. However, two chains that are bonded in the α configuration do not have any attraction between their tails, and these clusters are likely to break up instead of growing. The energies for bonded two-particle clusters are $U_\alpha = -0.5$ and $U_\beta = -0.74$, which translate into respective lifetimes $\tau_{2,\alpha} = 2.0 \times 10^5$ and $\tau_{2,\beta} = 6.9 \times 10^7$ at this temperature (recall that these times are given in MC steps). Growth of either phase requires that small clusters are stable for sufficiently long times that incoming particles can arrive and bind before these clusters disappear. The increased lifetime of two-particle β clusters promotes the formation of this phase, at short times. It gives rise to a linear coverage dependence of the β phase already for very short times. In contrast, stable α clusters need to be larger in order to become stable.

We note in passing that the slow onset of the growth of the α state is familiar from other contexts. In the classical nucleation of crystals, an initial slow nucleation step is followed by rapid growth [18]: one observes that the rate of crystal production $dN_{\rm xtal}/dt$ is a strongly increasing function of time t. Similar behavior is found (for example) in nucleated filament growth [19] and in self-assembly of viral capsids [20]. These processes share an initial slow step in the self-assembly process, after which the assembled structures grow more quickly. Here, the slow step is the formation of a cluster of the α phase that is large enough to be stabilized by tail-tail interactions.

The second feature that is clear from Fig. 7 is the strong increase of $N_{2\alpha}(\Theta)$ for $\Theta \geqslant 0.2$. This compensates for the slow initial growth of the α phase and gives rise to the final result $N_{2\alpha} > N_{2\beta}$ for $\Theta = 0.8$. Naturally, a cluster can only grow if binding sites are available: recall that $N_{1\alpha}^f$ measures the number of these binding sites. The growth of a cluster thus can be formally seen as a transformation of a chain that contributes to $N_{1\alpha}^f$ into a chain that contributes to $N_{2\alpha}$. One might expect that the probability for this transformation is proportional to $N_{1\alpha}^f$.

To analyze the impact of the number of free cluster chains $N_{1\alpha}^f$ on the rate of increase of the cluster, we have performed 350 independent simulations for $T = 0.041$ and $F = 6.7 \times 10^{-6}$ and determined the increase of $N_{2\alpha}$ when comparing its value for $\Theta = 0.21 + x$ with $\Theta = 0.2 + x$, where x is chosen as $0.00, 0.01, \ldots, 0.05$. In Fig. 8 this increase, denoted as $\Delta N_{2\alpha}$, is plotted vs $N_{1\alpha}^f$ as a scatter plot.

Obviously, a nonlinear behavior is observed. Here we use a power law $dN_{2\alpha}/d\Theta \sim (N_{1\alpha}^f)^a$ for a quantification of the observed sublinear dependence. Other fits would be possible as well. We take $a = 0.5$, consistent with the data in Fig. 8. In the following we concentrate on the α phase.

It is useful to define $P_\alpha^{\rm dis} \equiv N_{1\alpha}^f / N_\alpha$, which measures the fraction of α chains that are free for binding. Together with the power-law dependence noted above, we arrive at

$$\frac{dN_{2\alpha}}{d\Theta} = \Gamma_\alpha^{\rm eff} \left[P_\alpha^{\rm dis}\right]^{0.5} N_\alpha^{0.5}, \qquad (1)$$

where $\Gamma_\alpha^{\rm eff} \equiv (dN_{2\alpha}/d\Theta)/[N_{1\alpha}^f]^{0.5}$ is an effective growth rate. (For fixed particle densities, it is natural to assume that this rate

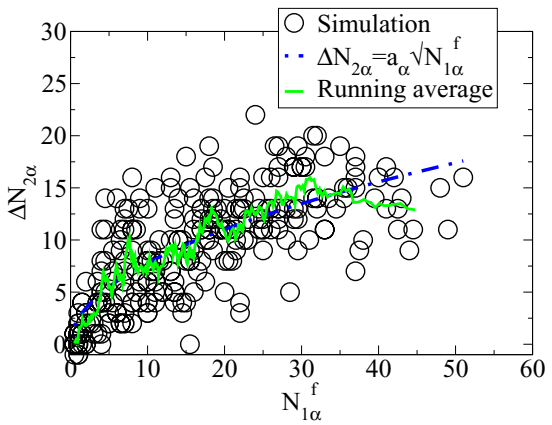

FIG. 8. (Color online) Increase of $\Delta N_{2\alpha}$ as a function of $N_{1\alpha}^f$. This demonstrates how the increase of chains with two α bonds depends on the availability of free chains. The solid line represents a least-squares fit of $\Delta N_{2\alpha} \propto [N_{1\alpha}^f]^a$ with $a = 0.48$. Furthermore, the running average is displayed.

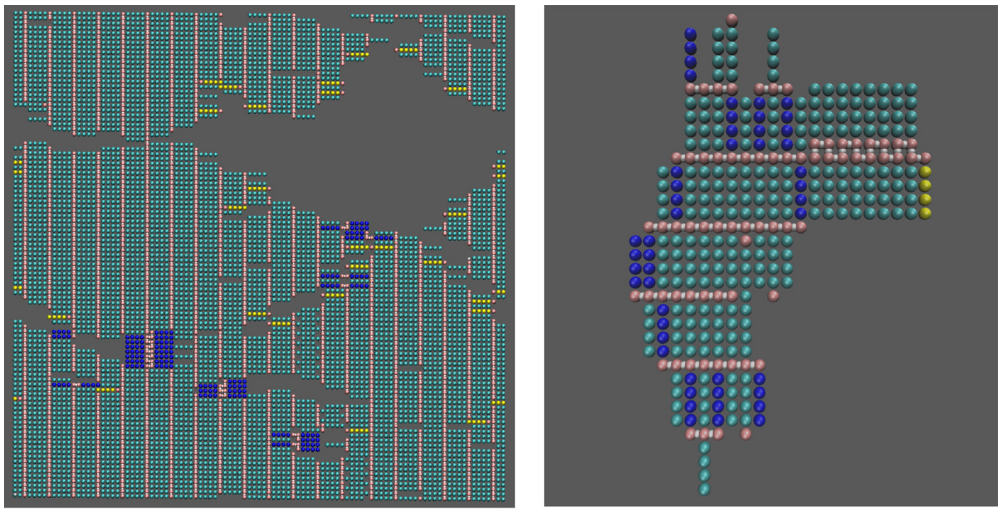

(a) (b)

FIG. 9. (Color online) Two typical configurations during the simulation. Left: α-rich domain. The few β chains are colored in the darker blue. Right: high-resolution image where the free chains are specifically highlighted (blue: free α-chains, green: free β-chains).

equation is independent of system size, in which case $\Gamma_\alpha^{\rm eff}/L$ is independent of system size. This is the quantity that we report in the following.)

To rationalize the growth kinetics, we consider separately the physical interpretations of the nontrivial exponent $a = 0.5$ and the typical values of the variable $P_\alpha^{\rm dis}$. To understand the nontrivial exponent (or equivalently, the sublinear dependence of $dN_{2\alpha}/d\Theta$ on $N_{1\alpha}^f$), we consider the spatial distribution of α chains (see Fig. 9). Growth of the α phase proceeds through extended (two-dimensional) clusters, with free chains distributed on their boundary, while the β phase grows as linear clusters, with free chains at their ends. It follows that free α chains tend to occur in localized regions of space, while free β chains are more uniformly distributed. On depositing a chain at a random position, the probability to encounter a free α chain is thus less than proportional to $N_{1\alpha}^f$.

Furthermore, as shown in Fig. 10, $P_\alpha^{\rm dis}$ is approximately 1 order of magnitude larger than $P_\beta^{\rm dis}$. A typical example at intermediate coverage is shown in Fig. 9. This reflects the fact that the surface of a two-dimensional α cluster of size $\mathcal{N} = \ell^2$ scales as $\ell = \sqrt{\mathcal{N}}$, while the "free surface" of a linear β cluster is of size of order unity, whatever the cluster size. Hence as clusters grow, the number of free α sites increases while the number of free β sites remains constant. This is an important kinetic factor in favor of the more rapid growth of α clusters as the coverage increases.

Interestingly, $P_\alpha^{\rm dis}$ displays only a minor dependence on coverage. The same holds for $\Gamma_\alpha^{\rm eff}$ (data not shown). Thus the relation $\frac{dN_{2\alpha}}{d\Theta} = \Gamma_\alpha^{\rm eff}[P_\alpha^{\rm dis}]^{0.5} N_\alpha^{0.5}$ implies that $dN_{2\alpha}/d\Theta \approx dN_\alpha/d\Theta \propto N_\alpha^{0.5}$. Using that for high coverage $N_\alpha \approx N_{2\alpha}$, this differential equation yields $N_\alpha(\Theta) \propto \Theta^2$. This relation is numerically verified in Fig. 11.

C. Understanding the dependence on flux

We now turn to the unusual dependence of the assembly process on flux; recall Fig. 6. In order to elucidate the underlying mechanisms, we first compare the Θ dependence for the highest and lowest flux in Fig. 6(d). The results are shown in Fig. 7.

These data show that for $\Theta = 0.05$, the average value of N_α decreases from 7 to 4, as the flux decreases. Thus the initial growth of an α cluster is hampered more strongly for lower

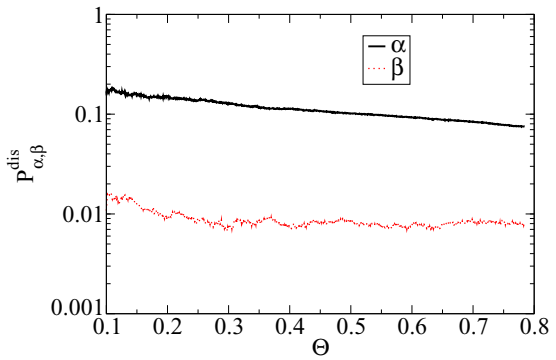

FIG. 10. (Color online) $P_{\alpha,\beta}^{\rm dis}$ is shown as a function of coverage at $T = 0.041$ and $F = 6.7 \times 10^{-6}$.

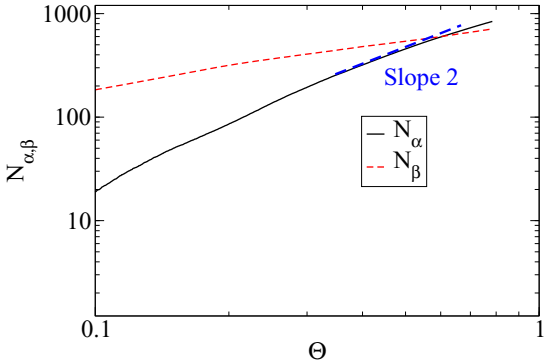

FIG. 11. (Color online) $N_{\alpha,\beta}$ is plotted as a function of Θ in a double-logarithmic representation. Included is a line of slope 2.

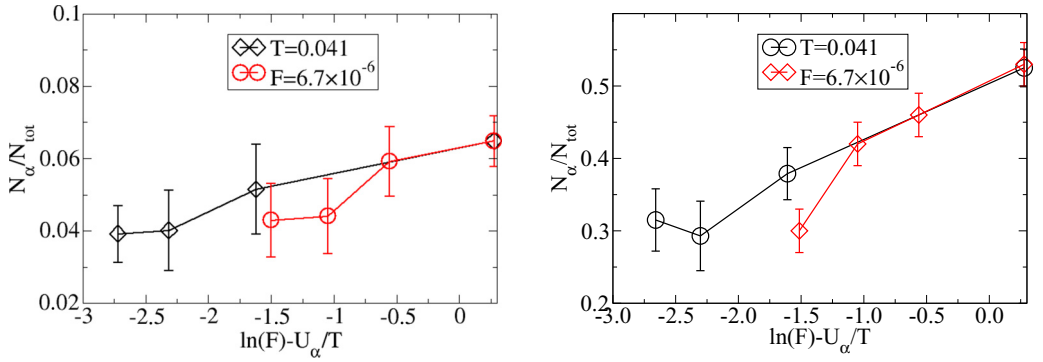

FIG. 12. (Color online) N_α is shown as a function of $\ln(F \times \tau_{2\alpha})$. One can see in a unified way how the fraction of α chains depends on the product of the α-cluster lifetime and the flux. Shown are $\Theta = 0.05$ (left) and $\Theta = 0.8$ (right).

flux. This can be rationalized by considering an small cluster of two chains that may either grow or shrink. The cluster lifetime is approximately $\tau_{2\alpha} = \exp(-U_\alpha/T)$: we estimate that the cluster will grow if a third chain attaches within this lifetime. The probability of such an event is approximately $F \times \tau_{2\alpha}$. Using this scaling variable allows unification of the temperature dependence and the flux dependence of this process. Indeed, as shown in Fig. 12, plotting the data in Figs. 6(b) and 6(d) in a single plot as a function of $\ln(F \times \tau_{2\alpha})$, both graphs agree semiquantitatively for low as well as for high coverage.

To discuss the behavior for intermediate coverage we study $\Gamma_\alpha^{\rm eff}$ and $P_\alpha^{\rm dis}$ (see Fig. 13). It turns out that $\Gamma_\alpha^{\rm eff}$ is basically flux independent, while $P_\alpha^{\rm dis}$ displays a significant flux dependence. Comparing the two extreme flux values, the value of $P_\alpha^{\rm dis}$ decreases by more than 30%. Recalling that $P_\alpha^{\rm dis}$ is related to the amount of surface in a typical cluster, this dependence can be accounted for because lower fluxes allow more time for local cluster rearrangements during the growth process. This gives rise to clusters with lower enthalpy and correspondingly fewer surface chains, and smaller values of $P_\alpha^{\rm dis}$. As a consequence, Eq. (1) predicts a weaker increase of the α phase for intermediate and large coverage. Thus, not only the initial cluster formation but also the cluster growth is less favorable for the α phase when decreasing the flux at this temperature.

D. Understanding the approach to equilibrium

As noted in previous sections, one expects that in the limit of very low flux the equilibrium behavior should be recovered. This expectation assumes that during the experimental (or simulation) time scale the system has sufficient time to explore all possible configurations so that it can indeed experience the lower enthalpy of the extended α phase. For $T = 0.041$ the flux required to observe this regime is so slow that it is inaccessible to our simulations. Otherwise the system does not have sufficient time to explore a sufficient number of different configurations, due to the slow time scales associated with thermal activation in this system.

In Fig. 14 we show the flux dependence of $N_\alpha/N_{\rm tot}$ for the higher temperature, $T = 0.057$, for several different values of the coverage Θ. Most interestingly, the fraction of the α phase first decreases but then, for even lower flux, increases again [see also Fig. 6(f)]. In this case, one can indeed observe the approach to thermodynamic equilibrium, although the naive estimate (see Sec. 5.1 above) for the equilibrium fraction of the α phase at this temperature is 0.94, which is still much higher than the value observed for the lowest flux.

For $\Theta = 0.05$ the nonmonotonicity of the yield $N_\alpha/N_{\rm tot}$ is much weaker in Fig. 14, indicating that this effect is not related to the short-time effects described in previous sections, which favor the formation of β over α structures at short times. The

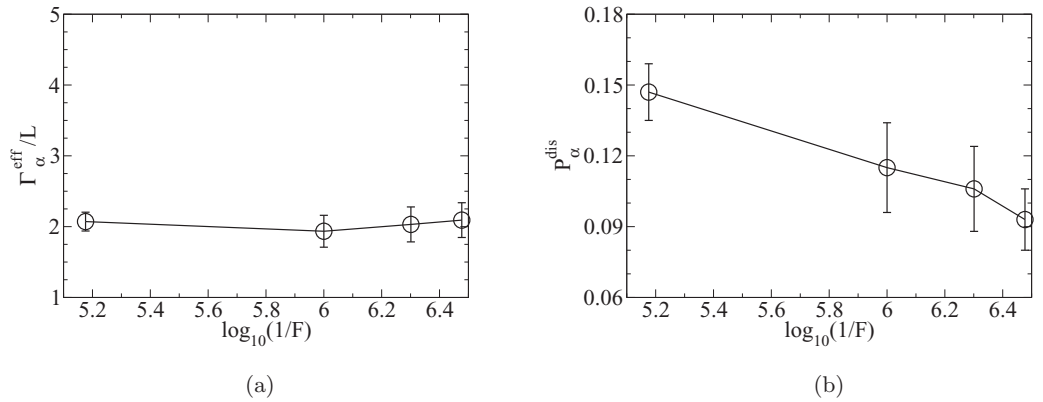

FIG. 13. (a) $\Gamma_\alpha^{\rm eff}$ and (b) $P_\alpha^{\rm dis}$ as a function of flux at $T = 0.041$ and $\Theta = 0.20$. Whereas $\Gamma_\alpha^{\rm eff}/L$ reflects the normalized growth rate of α clusters, $P_\alpha^{\rm dis}$ is the probability that an α chain is free, i.e., can be used as a site for an additional attachment.

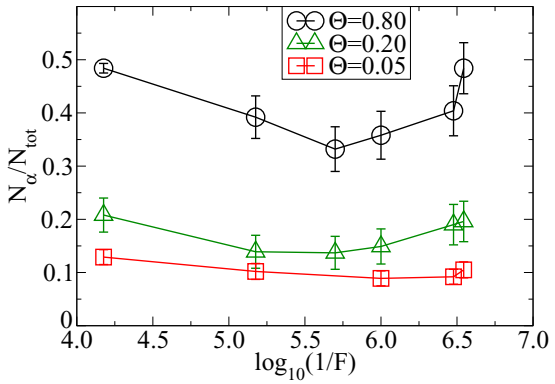

FIG. 14. (Color online) N_α is shown as a function of F at $T = 0.057$ for three different coverages $\Theta = 0.05$, $\Theta = 0.2$, and $\Theta = 0.8$.

origin of the nonmonotonicity in Fig. 14 is different, arising from the transformation of β clusters back into α as the system explores its configuration space and reaches the low-enthalpy α phase.

To quantify this effect we labeled all β chains at coverage $\Theta = 0.20$ and checked how many of these chains transform into α chains during the simulation. The fraction that does convert is denoted by $n_{\beta\alpha}$: results are shown in Fig. 15. First one observes a dramatic difference between both temperatures. For $T = 0.041$ the transformation from β to α is almost irrelevant, but for $T = 0.057$ a significant fraction of β chains indeed become α chains. The presence of this growth channel thus turns out to be a key requirement for the total system to approach thermodynamic equilibrium. This mechanism is important for $F \lesssim 10^{-5}$. Recall that for the larger fluxes in Fig. 14, the yield N_α/N_{tot} is reduced by reducing flux due to the mechanism discussed in the previous section. However, the conversion of β to α clusters seems to counterbalance this effect when the flux gets small, leading to the minimum in Fig. 14 at $F \approx 2.5 \times 10^{-6}$.

The parameter range for which this new growth channel is relevant can be estimated on general grounds. For a lamellar β cluster, the binding energy of the chain at the boundary is $U_\beta = -0.74$. This interaction energy takes into account the

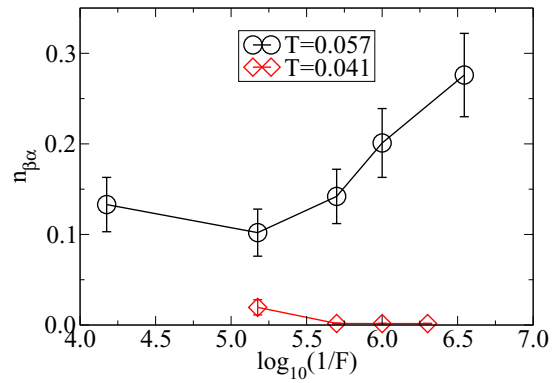

FIG. 15. (Color online) Transition probability from the β cluster to the α cluster during the interval of coverage $\Theta = 0.2$ and $\Theta = 0.8$ at two different temperatures $T = 0.041$ and $T = 0.057$.

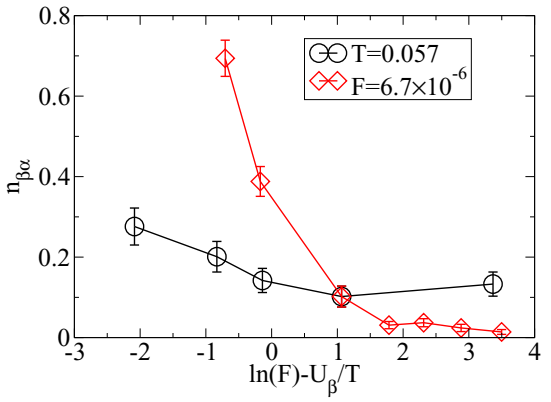

FIG. 16. (Color online) Transition probability from β to α is shown as a function of $F\exp(-U_\beta/T)$.

bond between head particles as well as the tail-tail interaction, (see Sec. 3 above). Thus, the time scale to leave the cluster is approximately $\exp(-U_\beta/T)$. Again, this time scale has to be compared with the inverse flux $1/F$, giving rise to the definition of a crossover flux $F_c(T) = \exp(U_\beta/T)$. For $F < F_c$ this chain has sufficient time to leave the cluster; in the opposite limit the cluster will grow due to the frequent advent of new chains. For $T = 0.057$ one finds $F_c \approx 10^{-5.6} = 2.510^{-6}$, which is very close to the value in Fig. 15 where $n_{\beta\alpha}$ starts to increase.

In the same spirit as in Sec. IV C the normal regime at high T and low F may be expected to depend on $F\exp(-U_\beta/T)$. This dependence should be most relevant for $n_{\beta\alpha}$, i.e., the probability that an initially formed β chain finally ends as an α chain. In Fig. 16 $n_{\beta\alpha}$ is shown as a function of $\ln[F\exp(-U_\beta/T)]$. Qualitatively, the simulations, originating from variation of T and F, respectively, display a significant decrease for low flux [normal regime where $F\exp(-U_\beta/T) < 1$] and become roughly constant (and small) in the opposite limit. Naturally, the final transition of a β chain to an α chain is a highly complex process which, strictly speaking, will depend on flux and temperature individually. Nevertheless, the qualitative agreement in Fig. 16 suggests that the initial escape of β chains from their respective cluster plays an important role in the equilibration process. In particular, this intimate relation between flux and temperature rationalizes why the nonmonotonous flux dependence translates into a nonmonotonous temperature dependence, as seen experimentally and numerically in Fig. 6.

V. DISCUSSION

Monte Carlo simulations are based on a simple model where substituted adenine derivatives are coarse grained by rigid head-tail chain molecules with five beads. Of course, the present model could be further optimized to become even closer to the experimental data. For example, entropic effects, reflecting the flexibility of the binding of two adjacent chains, might be included. However, since our goal was to find a (close to) minimum model to reproduce the experimental observations, we restricted ourselves to the consideration of the topological effects.

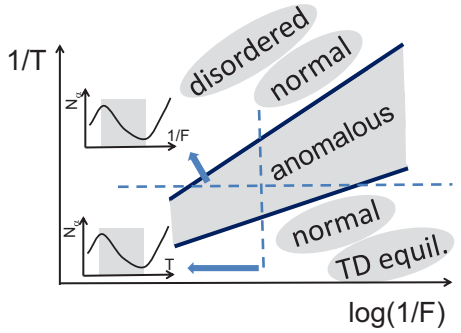

FIG. 17. (Color online) Sketch of the nonequilibrium behavior in dependence of T and F. The solid lines correspond to the two crossover flux values, defined by $F\exp(-U_\alpha/T)$ and $F\exp(-U_\beta/T)$, respectively, as discussed in the text. The anomalous regime is highlighted. The T- and F-dependent curves of N_α, shown on the left and the bottom of the figure, respectively, would have been measured along the broken lines.

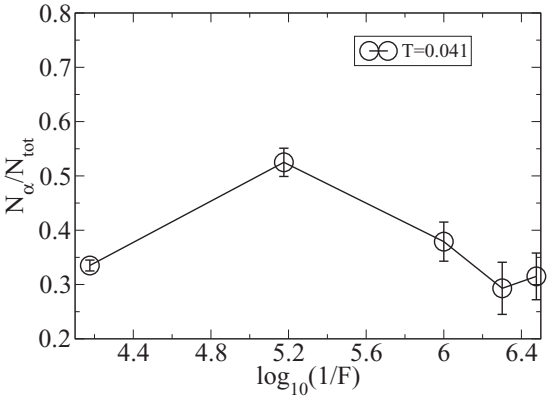

FIG. 18. Extending the flux range of Fig. 5(d) to an even higher flux value.

A. Summary of mechanisms and relevant time scales

We have studied the structure formation of substituted adenine derivative on surfaces experimentally as well as numerically. The simulation model can numerically reproduce the two phases found in the experiment and the observed dependence of the "yield" on flux and temperature. We have identified two key mechanisms: (i) For $F\exp(-U_\alpha/T) \leqslant 1$, two-particle clusters of the α phase typically dissociate before growing into three-particle clusters: this effect favors formation of the β phase (recall Fig. 12). The difference between the phases arises from the absence of attractive forces between the molecules' tails in the two-particle α cluster, so that the interaction energy U_α corresponds to an interaction only between head particles. (ii) For $F\exp(-U_\beta/T) \leqslant 1$, bonds within β clusters are weak enough that thermal fluctuations can break them during the growth process, which allows efficient exploration of configuration space and favors the α phase. Here the energy scale of $U_\beta = -0.74$ describes the energy which is required to remove one chain from a β cluster.

In the temperature-flux regime $\exp(-U_\beta/T) \geqslant 1/F \geqslant \exp(-U_\alpha/T)$, we find unusual nonequilibrium effects on the yield $N_\alpha/N_{\rm tot}$ of the nonequilibrium assembly process. This parameter regime is sketched in Fig. 17. As a consequence, the condition to see this anomalous behavior is that the head-head interaction for an α bond is smaller than the binding energy of a chain at the boundary of a lamellar β cluster. Also sketched is the regime where thermodynamic equilibrium is closely approached (low flux, high temperature).

In the third regime (high flux, low temperature) we observe that the system displays the very same behavior as for very low flux, i.e., more α phase for lower flux; see Fig. 18. This is fully consistent with our general theoretical considerations and is also included in Fig. 17. Since, however, this third regime cannot be accessed experimentally, we do not dwell on this question in more detail. Of course, finally at very high flux and very low temperature the structure formation starts to cease and disordered structures are observed.

For the experimentally used flux values, the transition between the anomalous and the normal flux dependence is observed for $T \approx 330$ K, corresponding to $T \approx 0.028$ in units of eV. In contrast, the transition temperature for the simulations is close to 0.05. Since the energy of the adenine chain has been estimated from DFT calculations, a semiquantitative comparison between experiment and simulation should be possible. Indeed, this difference can be (qualitatively) related to the different time scales. Since the transition is roughly governed by the relation $\exp(-U_\beta/T) \approx 1/F$ and using $U_\beta = -0.74$ we obtain $(F_{\rm sim}/F_{\rm exp}) \approx 10^5$. Experimentally, the substrate is covered after approximately 20 min, which we approximate as 10^3 s. Numerically, the corresponding coverage is reached after approximately 10^5 Monte Carlo steps. One Monte Carlo step corresponds to the diffusive dynamics of the adenine molecule by one model unit, corresponding to about 5 carbon atoms, which we approximate as 1 nm. Unfortunately, the experimental diffusion constant is not known. For lipophilic molecules diffusion values are reported in the range $10^{-1} - 10^{-3}$ nm^2/ns [21]. Somewhat larger diffusion constants (10^0 nm^2/ns) are reported for the diffusion of small n-alkanes on surfaces [22]. Thus it may be consistent for our very rough approximation to choose $D = 10^{-2}$ nm^2/ns, and the elementary time step is 10^{-8} s. Thus the length of the simulation corresponds to $10^5 \times 10^{-8}$ s $= 10^{-3}$ s. This would differ by 6 orders of magnitude from the experimental time scale. This difference is not too far away from the 5 orders of magnitude estimated from the differences in temperature. Thus, on a qualitative level, the simulations and the experiments are fully consistent with respect to the different temperatures.

B. Relation to other self-assembling systems

Analyzing this molecular self-assembly process from a more abstract viewpoint (see, for example, Ref. [17]), the most important effect is that for small clusters of the α and β phases, the lowest free energy state is the β cluster. It is only for larger clusters that the lower bulk free energy of the α phase becomes apparent.

This scenario gives rise to different regimes of self-assembly and kinetic trapping. Starting from a very high flux, the initial clusters are formed randomly and naturally form kinetic traps in which the corresponding chains are trapped during the short time of the experiment or simulation. For intermediate flux the kinetic trapping becomes more complex. Now

the system has sufficient time to realize that for small clusters the β phase is thermodynamically more stable, particularly for very low flux. As a consequence, the formation of the α phase is more and more suppressed with decreasing flux. Only if the flux is further decreased does the system have sufficient time to explore configuration space to arrive in the thermodynamically stable α phase after starting from the β phase.

In self-assembly, similar observations have been recently made for the structure formation of one-patch colloids [23,24]. For an appropriately chosen patch coverage, both tubelike and lamellar structures are observed, where the lamellar structure is thermodynamically stable. However, for low temperatures and low densities, tubelike structures are dominating the self-assembly process. As in the case considered here, quasi-one-dimensional structures tend to be associated with lower surface costs so they may be more stable for small clusters—both tubelike structures and the β phase considered here have this property. Analyzing our data for low but not too low coverage, e.g., $\Theta = 0.20$, the β phase does indeed dominate even at very low flux, due to this kinetic effect. Whereas in Refs. [23,24] these metastable states are somewhat a nuisance for the determination of high-quality equilibrium phase diagrams, in the present work we are particularly interested in the nonequilibrium nature of deposition experiments and simulations and thus can analyze the complex approach to equilibrium in dependence of flux and temperature.

In the classical case of phase transitions, the idea that a state with low surface cost may nucleate in preference to the thermodynamically stable state is related to the conjecture of Stranski and Totomanow, since lower surface costs are associated with lower nucleation barriers (see, for example, Refs. [25] and [17]). The result is that metastable crystals may nucleate in preference to minimal free-energy structures. This analogy, and the link to one-patch colloids, both emphasize the generic nature of the nonequilibrium phenomena that are reported here in deposition experiments.

ACKNOWLEDGMENT

We greatly appreciate and acknowledge support by the DFG via Projects No. TRR 61 and No. SFB 858.

P.K.J. and C.W. contributed equally to this work.

[1] Stephen R. Forrest, Ultrathin organic films grown by organic molecular beam deposition and related techniques, Chem. Rev. **97**, 1793 (1997).

[2] Zheng-Tao Zhu, Jeffrey T. Mason, Ruediger Dieckmann, and George G. Malliaras, Humidity sensors based on pentacene thin-film transistors, Appl. Phys. Lett. **81**, 4643 (2002).

[3] John A. Rogers, Zhenan Bao, Kirk Baldwin, Ananth Dodabalapur, Brian Crone, V. R. Raju, Valerie Kuck, Howard Katz, Karl Amundson, Jay Ewing, and Paul Drzaic, Paper-like electronic displays: Large-area rubber-stamped plastic sheets of electronics and microencapsulated electrophoretic inks, Proc. Natl. Acad. Sci. USA **98**, 4835 (2001).

[4] David Voss, Cheap and cheerful circuits, Nature (London) **407**, 442 (2000).

[5] Y Karzazi, Organic light emitting diodes: Devices and applications, J. Mater. Environ. Sci. **5**, 1 (2014).

[6] Mang Mang Ling and Zhenan Bao, Thin film deposition, patterning, and printing in organic thin-film transistors, Chem. Mater. **16**, 4824 (2004).

[7] T. Michely and J. Krug, *Islands, Mounds and Atoms* (Springer-Verlag, Berlin, 2004).

[8] W. C. Wang, D. Y. Zhong, J. Zhu, F. Kalischewski, R. F. Dou, K. Wedeking, Y. Wang, A. Heuer, H. Fuchs, G. Erker, and L. F. Chi, Patterned Nucleation Control in Vacuum Deposition of Organic Molecules, Phys. Rev. Lett. **98**, 225504 (2007).

[9] R. Vardavas, C. Ratsch, and R. E. Caflisch, Submonolayer growth in the presence of defect sites, Surf. Sci. **569**, 185 (2004).

[10] Fabian Lied, Tanja Mues, Wenchong Wang, Lifeng Chi, and Andreas Heuer, Different growth regimes on prepatterned surfaces: Consistent evidence from simulations and experiments, J. Chem. Phys. **136**, 024704 (2012).

[11] Stefan Frieder Hopp and Andreas Heuer, Anisotropic behavior of organic molecules on prepatterned surfaces, J. Chem. Phys. **136**, 154106 (2012).

[12] Raffaela Cabriolu, Dimo Kashchiev, and Stefan Auer, Breakdown of nucleation theory for crystals with strongly anisotropic interactions between molecules, J. Chem. Phys. **137**, 204903 (2012).

[13] Mohit Haran, Joseph E. Goose, Nicolas P. Clote, and Paulette Clancy, Multiscale modeling of self-assembled monolayers of thiophenes on electronic material surfaces, Langmuir **23**, 4897 (2007).

[14] Kenneth L. Kearns, Stephen F. Swallen, M. D. Ediger, Tian Wu, Ye Sun, and Lian Yu, Hiking down the energy landscape: Progress toward the Kauzmann temperature via vapor deposition, J. Phys. Chem. B **112**, 4934 (2008).

[15] Can Wang, Pritam Kumar Jana, Haiming Zhang, Zhongcheng Mu, Gerald Kehr, Tobias Blomker, Gerhard Erker, Harald Fuchs, Andreas Heuer, and Lifeng Chi, Controlling two-phase self-assembly of an adenine derivative on HOPG via kinetic effects, Chem. Commun. **50**, 9192 (2014).

[16] Zhongcheng Mu, Oliver Rubner, Markus Bamler, Tobias Blmker, Gerald Kehr, Gerhard Erker, Andreas Heuer, Harald Fuchs, and Lifeng Chi, Temperature-dependent self-assembly of adenine derivative on HOPG, Langmuir **29**, 10737 (2013).

[17] S. Whitelam and R. L. Jack, The Statistical Mechanics of Dynamic Pathways to Self-Assembly, Ann. Rev. Phys. Chem. **66**, 143 (2015).

[18] R. P Sear, Quantitative studies of crystal nucleation at constant supersaturation: Experimental data and models, Cryst. Eng. Comm. **16**, 6506 (2014).

[19] T. P. J. Knowles *et al.*, An analytical solution to the kinetics of breakable filament assembly, Science **326**, 1533 (2009).

[20] M. F. Hagan and O. M. Elrad, Understanding the concentration dependence of viral capsid assembly kinetics—The origin of the lag time and identifying the critical nucleus size, Biophys. J. **98**, 1065 (2010).

[21] Lukas Schreiber, Review of sorption and diffusion of lipophilic molecules in cuticular waxes and the effects of accelerators on solute mobilities, J. Exp. Bot. **57**, 2515 (2006).

[22] Yehuda Zeiri, Molecular dynamics study of the surface diffusion of large adsorbates: III. Role of adsorbate shape, Can. J. Chem. **72**, 813 (1994).

[23] Zdenek Preisler, Teun Vissers, Frank Smallenburg, Gianmarco Muna, and Francesco Sciortino, Phase diagram of one-patch colloids forming tubes and lamellae, J. Phys. Chem. B **117**, 9540 (2013).

[24] Gianmarco Munao, Zdenek Preisler, Teun Vissers, Frank Smallenburg, and Francesco Sciortino, Cluster formation in one-patch colloids: Low coverage results, Soft Matter **9**, 2652 (2013).

[25] L. O. Hedges and S. Whitelam, Limit of validity of Ostwald's rule of stages in a statistical mechanical model of crystallization, J. Chem. Phys. **135**, 164902 (2011).